

Blind Source Separation of Radar Signals in Time Domain Using Deep Learning

Sven Hinderer^{*†}

^{*}Fraunhofer Institute for High Frequency Physics and Radar Techniques FHR, 53343 Wachtberg, Germany

[†]Institute of Signal Processing and System Theory, University of Stuttgart, 70569 Stuttgart, Germany

sven.hinderer@fhr.fraunhofer.de

sven.hinderer@iss.uni-stuttgart.de

Note: This is the accepted version of the paper. The final version is published in the *Proceedings of the IEEE 2022 23rd International Radar Symposium (IRS)*. DOI: 10.23919/IRS54158.2022.9904990

Abstract—Identification and further analysis of radar emitters in a contested environment requires detection and separation of incoming signals. If they arrive from the same direction and at similar frequencies, deinterleaving them remains challenging. A solution to overcome this limitation becomes increasingly important with the advancement of emitter capabilities. We propose treating the problem as blind source separation in time domain and apply supervisedly trained neural networks to extract the underlying signals from the received mixture. This allows us to handle highly overlapping and also continuous wave (CW) signals from both radar and communication emitters. We make use of advancements in the field of audio source separation and extend a current state-of-the-art model with the objective of deinterleaving arbitrary radio frequency (RF) signals. Results show, that our approach is capable of separating two unknown waveforms in a given frequency band with a single channel receiver.

Index Terms—Deep Learning, Transformer, Source Separation, Cognitive Radar, Electronic Support, Low Probability of Intercept

I. INTRODUCTION

An important task in the field of passive surveillance is the analysis of hostile radar emitters to estimate their mode of operation, their potential threat level, and to gain situational awareness. In a modern Electronic Warfare (EW) environment, we usually receive multiple signals from different radio emitters simultaneously. It is therefore required to separate these signals and assign them to their emitters before applying further signal processing operations.

As of now, this problem is solved by first separating radar and communication signals. Radar signals are further divided into pulsed and CW signals. Pulsed radar signals are described by pulse descriptor words (PDWs) and the extracted radar signal parameters are used to represent emitters with emitter descriptor words (EDWs). Pulse parameters to describe

radar signals are e.g. the time of arrival (TOA), pulse width (PW), angle of arrival (AOA), pulse amplitude (PA) and RF. A comparison of various popular approaches to deinterleave the extracted train of PDWs can be found in [1]. Newer literature solves the problem with self-attention based soft min-cost flow learning, showing promising results [2].

Although these deinterleaving approaches work well and are able to separate pulse trains under difficult conditions, they might fall short in separating signals in more complex scenarios. These include separation of not only pulsed, but also CW signals from both radar and communication emitters with a single channel receiver or if they originate from the same direction, dealing with pulses widely spread in frequency and time and also detecting and separating them under low signal-to-noise ratio (SNR) conditions.

We propose treating the problem as blind source separation and use deep neural networks to separate the raw baseband input mixture in time domain. Blind source separation is an ongoing research topic, where huge advancements have been made over the last years by using deep neural networks [3]–[6]. Since this approach makes no assumptions about the inputs besides them being in the frequency band of interest, it is able to handle the aforementioned shortcomings of current methods. It comes, however, at the cost of high computational complexity and the need for extensive training data to achieve good separation performance. In this first study, we restrict us to a single input channel and two superposed signals. We adapt ideas from state-of-the-art neural network architectures in the field of single channel audio source separation to separate RF signals that can overlap in frequency and time. This is done by estimating two filter masks, which divide the mixed input into two separate components.

II. MODEL

A. Overview

An overview of the RF signal separation system is shown in Fig. 1. To handle the bandwidth of received signals and their amplitudes' dynamic range, which are much larger for RF signals than what is investigated in the audio domain, multiple novel elements are added to the processing chain. These include differentiable short-time Fourier transforms (STFTs) and inverse short-time Fourier transforms (iSTFTs) instead of 1D convolutional layers, since they are very fast by

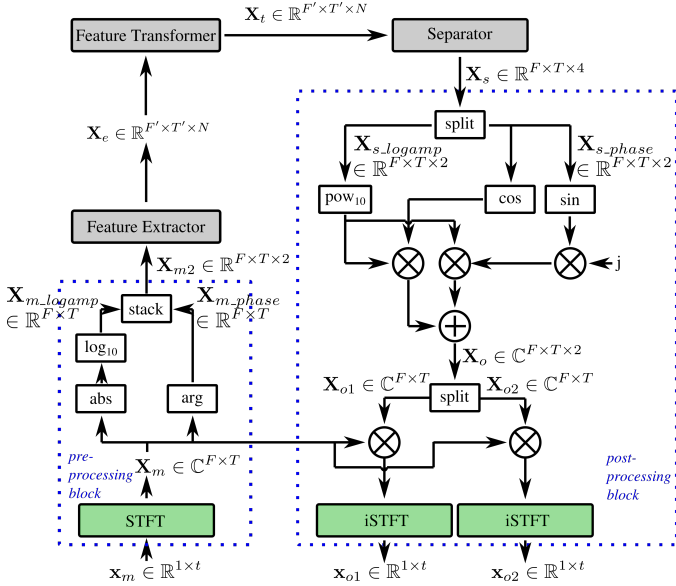


Fig. 1: Overview of the whole system: In the preprocessing, we convert the superposition of signals from time domain to time-frequency domain and apply transformations to handle the dynamic range of amplitudes. The processed input is then fed to our three trainable network modules. The predicted masks from the Separator are transformed again in the postprocessing stage, multiplied with the input mixture in time-frequency domain and the resulting separated signals are converted back to time domain.

applying the fast Fourier transform (FFT) and inverse fast Fourier transform (iFFT) algorithms. They are also strictly information preserving with appropriate settings, commonly used to represent RF data and allow for logarithmic amplitude transformations. The rest of our network is built around the proposed time-frequency processing with the main workload to estimate two masks for separating the input mixture into two components being done in the Feature Transformer module.

B. Preprocessing

The mixed input signal in time domain $\mathbf{x}_m \in \mathbb{R}^{1 \times t}$ is transformed into its time-frequency representation $\mathbf{X}_m \in \mathbb{C}^{F \times T}$ using the discrete STFT [7]

$$\mathbf{X}_m = \text{STFT}(\mathbf{x}_m), \quad (1)$$

where t is the number of time steps of the time domain signal and T and F are the number of time and frequency bins of its STFT. The complex STFT is then converted into its exponential form and by applying a \log_{10} -transform to the absolute values, the potentially very large dynamic range of input amplitudes from different signals is squeezed:

$$\mathbf{X}_{m_logamp} = \log_{10}(|\mathbf{X}_m|) \quad (2)$$

$$\mathbf{X}_{m_phase} = \text{atan2}(\Im(\mathbf{X}_m), \Re(\mathbf{X}_m)). \quad (3)$$

Through stacking the log-amplitude $\mathbf{X}_{m_logamp} \in \mathbb{R}^{F \times T}$ and phase information $\mathbf{X}_{m_phase} \in \mathbb{R}^{F \times T}$ along a new, third di-

mension, the 3D input tensor $\mathbf{X}_{m2} \in \mathbb{R}^{F \times T \times 2}$ for the Feature Extractor is formed.

C. Feature Extractor

The 3D input to the Feature Extractor is processed by a SeparableConv2D layer [8], [9] followed by Layer Normalization (LN) [10], building the intermediate Feature Extractor representation $\mathbf{X}_{e1} \in \mathbb{R}^{F' \times T' \times N}$, where N denotes the number of kernels in the convolution layer

$$\mathbf{X}_{e1} = \text{LN}(\text{SeparableConv2D}(\mathbf{X}_{m2})). \quad (4)$$

In the next step, another SeparableConv2D layer is applied to \mathbf{X}_{e1} , which allows for downsampling along the time and frequency axis by using strides > 1 . The convolution output is again normalized with LN and now nonlinearly activated with the Rectified Linear Unit (ReLU) [9]. The second Feature Extractor signal $\mathbf{X}_{e2} \in \mathbb{R}^{F' \times T' \times N}$ is therefore given by

$$\mathbf{X}_{e2} = \text{ReLU}(\text{LN}(\text{SeparableConv2D}(\mathbf{X}_{e1}))) \quad (5)$$

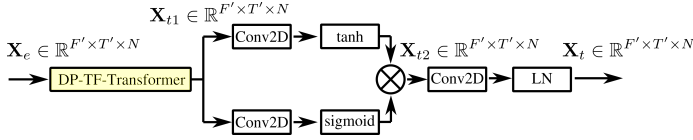
with new dimensions F' and T' , resulting from the strides in the convolution. The output of the Feature Extractor $\mathbf{X}_e \in \mathbb{R}^{F' \times T' \times N}$ is built by passing \mathbf{X}_{e2} through a Conv2D layer [8], [9] with subsequent LN since we realized, that adding another convolutional layer after downsampling improves accuracy:

$$\mathbf{X}_e = \text{LN}(\text{Conv2D}(\mathbf{X}_{e2})). \quad (6)$$

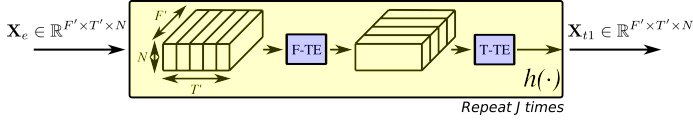
D. Feature Transformer

The Feature Transformer takes the Feature Extractor output and returns a block of the same shape. Its goal is to transform $\mathbf{X}_e \in \mathbb{R}^{F' \times T' \times N}$ into a representation $\mathbf{X}_t \in \mathbb{R}^{F' \times T' \times N}$ from which the mixed input can be separated effectively. A high level view of the Feature Transformer is shown in Fig. 2a. The main component of the Feature Transformer and also of our entire model, which we call Dual-Path Time-Frequency Transformer (DP-TF-Transformer), is closely related to the SepFormer block in [6], as it combines the parallelization and performance of Transformers [11] with the efficient long sequence modeling capabilities of dual-path processing introduced in [5]. The DP-TF-Transformer is described in Fig. 2b. It uses a stack of J modules, which are defined by the operation $h(\cdot)$. First comes a component we name Frequency Transformer Encoder (F-TE) that splits the input into T' frequency-channel-blocks of size $F' \times N$ and processes them separately. The F-TE applies a Transformer Encoder to each of these blocks. This Transformer Encoder attends to the frequencies and channels. The T' blocks which have passed through the F-TE are stacked together so that its input and output have equal shape. The same operation is then performed along the time instead of the frequency axis, where a Time Transformer Encoder (T-TE) processes F' time-channel-blocks of shape $T' \times N$ and concatenates all F' output blocks again. The mapping between DP-TF-Transformer input $\mathbf{X}_e \in \mathbb{R}^{F' \times T' \times N}$ and output $\mathbf{X}_{t1} \in \mathbb{R}^{F' \times T' \times N}$ can be described as

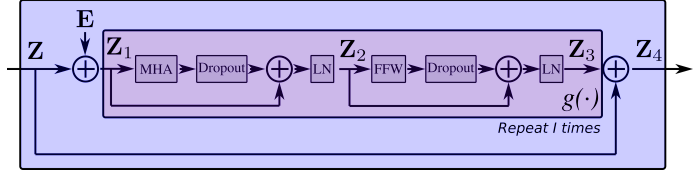
$$\mathbf{X}_{t1} = h^J(\mathbf{X}_e), \quad (7)$$



(a) The Feature Transformer block with DP-TF-Transformer in yellow and gated output processing.



(b) The DP-TF-Transformer, which consists of J stacks of F-TEs and T-TEs in series.



(c) Structure of the Transformer Encoders that process one block in the F-TEs and T-TEs. First, the positional encoding is added. Then, I stacks of vanilla Transformer Encoders follow. The input and output are connected by residual addition.

Fig. 2: Description of the Feature Transformer block.

where $h^J(\cdot)$ denotes J applications of DP-TF-Transformer modules. The Transformer Encoders used to process one block are presented in detail in Fig. 2c. We stick to the vanilla Transformer implementation [11] and add sinusoidal positional encodings $\mathbf{E} \in \mathbb{R}^{F' \times N}$ or $\mathbf{E} \in \mathbb{R}^{T' \times N}$ to the input $\mathbf{Z} \in \mathbb{R}^{F' \times N}$ or $\mathbf{Z} \in \mathbb{R}^{T' \times N}$ before each F-TE and T-TE block respectively

$$\mathbf{Z}_1 = \mathbf{Z} + \mathbf{E}. \quad (8)$$

Such encoding is required since Transformers, as opposed to e.g. recurrent neural networks (RNNs), have no intrinsic knowledge about the order of inputs. The encoded input of one block \mathbf{Z}_1 is put through a number of I Transformer Encoder layers, each implementing the operation $g(\cdot)$, as seen in the violet box of Fig. 2c. First, a Multi-Head Attention (MHA) layer [11], which performs scaled dot-product attention over the input with multiple heads, is employed. We then add Dropout [9], a residual addition around the MHA input and Dropout output and normalize with LN, resulting in \mathbf{Z}_2 :

$$\mathbf{Z}_2 = \text{LN}(\text{Dropout}(\text{MHA}(\mathbf{Z}_1)) + \mathbf{Z}_1). \quad (9)$$

\mathbf{Z}_2 is passed to a point-wise feed-forward (FFW) network [11], followed by Dropout, a residual addition around both operations and LN, which gives us \mathbf{Z}_3 with

$$\mathbf{Z}_3 = \text{LN}(\text{Dropout}(\text{FFW}(\mathbf{Z}_2)) + \mathbf{Z}_2). \quad (10)$$

The mapping from \mathbf{Z}_1 to \mathbf{Z}_3 defined by the function $g(\cdot)$ is repeated I times, before a residual addition around the whole block forms the output

$$\mathbf{Z}_4 = g^I(\mathbf{Z}_1) + \mathbf{Z}. \quad (11)$$

Note that the stack of blocks in an F-TE and T-TE is processed in parallel, which speeds up the architecture. The Transformer Encoders that operate on the different blocks in one of I layers also have shared weights, i.e. every block in such stack is processed with the same Transformer Encoder. This keeps the number of parameters and the computational complexity relatively low. At the head of our Feature Transformer, we apply a gating mechanism found in some audio models [12], [13] for 1D signals, that produces slight performance improvements. The gating output $\mathbf{X}_{t2} \in \mathbb{R}^{F' \times T' \times N}$ is calculated as

$$\begin{aligned} \mathbf{X}_{t2} &= \tanh(\text{Conv2D}(\mathbf{X}_{t1})) \circ \\ &\quad \text{sigmoid}(\text{Conv2D}(\mathbf{X}_{t1})), \end{aligned} \quad (12)$$

where \circ denotes the Hadamard product [9] and sigmoid and tanh [9] are activation functions. The final Feature Transformer output $\mathbf{X}_t \in \mathbb{R}^{F' \times T' \times N}$ then becomes

$$\mathbf{X}_t = \text{LN}(\text{Conv2D}(\mathbf{X}_{t2})). \quad (13)$$

E. Separator

In the Separator, the processed Feature Transformer output is first put through a Conv2DTranspose layer [14] with the same stride as the downsampling SeparableConv2D layer in the Feature Extractor module. Thereby, the frequency and time dimensions are upsampled to their original shape. We then normalize with LN and activate this output with ReLU, resulting in the intermediate Separator signal $\mathbf{X}_{s1} \in \mathbb{R}^{F \times T \times N}$ with

$$\mathbf{X}_{s1} = \text{ReLU}(\text{LN}(\text{Conv2DTranspose}(\mathbf{X}_t))). \quad (14)$$

For the estimation of wanted filter masks $\mathbf{X}_s \in \mathbb{R}^{F \times T \times 4}$, we employ a Conv2D layer with 4 kernels and linear activation:

$$\mathbf{X}_s = \text{Conv2D}(\mathbf{X}_{s1}). \quad (15)$$

The first half of \mathbf{X}_s are the log-amplitudes and the second half the phases of both masks.

F. Postprocessing

The log-amplitude and phase information from the Separator is then split. Log-amplitudes $\mathbf{X}_{s_logamp} \in \mathbb{R}^{F \times T \times 2}$ are converted back to amplitudes in linear scale $\mathbf{X}_{s_linamp} \in \mathbb{R}^{F \times T \times 2}$ using

$$\mathbf{X}_{s_linamp} = 10^{\mathbf{X}_{s_logamp}}. \quad (16)$$

With the amplitude and phase information $\mathbf{X}_{s_phase} \in \mathbb{R}^{F \times T \times 2}$, we can then construct the complex valued filter masks $\mathbf{X}_o \in \mathbb{C}^{F \times T \times 2}$ with

$$\begin{aligned} \mathbf{X}_o &= \mathbf{X}_{s_linamp} \circ \cos(\mathbf{X}_{s_phase}) + \\ &\quad \mathbf{X}_{s_linamp} \circ j \sin(\mathbf{X}_{s_phase}). \end{aligned} \quad (17)$$

By splitting \mathbf{X}_o along the last dimension, we get the STFT masks of the two signals $\mathbf{X}_{o1} \in \mathbb{C}^{F \times T}$ and $\mathbf{X}_{o2} \in \mathbb{C}^{F \times T}$. These are multiplied element-wise with the STFT of the

input mixture and the separated output signals in time domain $\mathbf{x}_{o1} \in \mathbb{R}^{1 \times t}$ and $\mathbf{x}_{o2} \in \mathbb{R}^{1 \times t}$ are formed by discrete iSTFT:

$$\mathbf{x}_{o1} = \text{iSTFT}(\mathbf{X}_{o1} \circ \mathbf{X}_m) \quad (18)$$

$$\mathbf{x}_{o2} = \text{iSTFT}(\mathbf{X}_{o2} \circ \mathbf{X}_m). \quad (19)$$

Since all operations of our network are differentiable, we can train the whole model end-to-end in time domain with backpropagation. Separating in time domain enables us to apply well established and powerful loss functions from the audio field, which circumvents the problem of finding suitable time-frequency losses.

III. EXPERIMENTS

A. Architecture Details

For the STFT and iSTFT, we use a Hann window [7] of size 512 with a hop size of 256 discrete time steps and therefore transform $\mathbf{x}_m \in \mathbb{R}^{1 \times 65280}$ into its time-frequency representation $\mathbf{X}_m \in \mathbb{C}^{257 \times 256}$, where we use only the positive frequency bins, which contain all information because \mathbf{x}_m is real-valued. The SeparableConv2D layers in the Feature Extractor and the Conv2DTranspose layer in the Separator have a kernel size of 4×4 , all Conv2D layers use 1×1 kernels. We set 2×2 strides for down- and upsampling in the corresponding convolutional Feature Extractor and Separator layers, which allows for a bigger model at the cost of compressing the signal in frequency and time. To avoid information loss in the downsampling operation, we add one zero-padded frequency bin beforehand. Consequently, the Separator output has the dimension $(F+1) \times T \times 4$ and we delete the last frequency component again to be able to multiply estimated masks with the mixed input. For simplicity, the feature dimension N is kept constant throughout the model. This includes the model- and inner feed-forward dimension of the Transformer Encoders and all convolutional layers except for the Separator output. We set $N = 128$ heuristically, such that the available Graphics Processing Unit (GPU) memory of 8 GB (Nvidia GeForce GTX 1080) is maxed out while training with a batch size of 2. MHA layers have 2 attention heads and we choose $I = J = 2$ for the DP-TF-Transformer with a dropout rate of 0.1 in the Dropout layers. For positional encoding, we stick to the original settings in [11]. Our model has 1.145.764 parameters in total.

B. Dataset

Datasets are created by simulating common Low Probability of Intercept (LPI) waveforms using GNU Radio [15] and Python. To evaluate the algorithm with both simulated and real signals, we transmit and receive all test samples with a software defined radio (SDR) in a simplistic setup, shown in Fig. 3. As intrapulse modulation, we choose P1, Costas and Frank codes [16] for training and P3, Barker and linear chirps [16] for testing. Interpulse modulations can be either CW, constant Pulse Repetition Interval (PRI), stagger PRI, jitter PRI or Dwell and Switch. Due to hardware limitations, a sample rate of 50 MHz is used and all signals are in the



Fig. 3: Simple setup for real data generation: Test samples are automatically transmitted and received by a SDR (USRP X310 by Ettus) as seen on the right. The channel is a cable with a 6 dB attenuator.

frequency range between 0 MHz and 25 MHz, an extension to shift this to an arbitrary band would however be straight forward.

For each intrapulse modulation type, we generate 2000 samples for training and 1000 for testing with a length of 10^6 time steps. To increase the variance of the dataset, which is necessary to achieve a high level of generalization of the trained neural network, we randomly choose a new set of parameters each sample. These are described in Table I.

TABLE I
INTRAPULSE PARAMETERS OF THE USED WAVEFORMS. SAMPLES ARE DRAWN UNIFORMLY FROM GIVEN VALUES OR VALUE RANGES.

Intrapulse modulation	Parameters	Values
All	PW	[4, 50) μs
	PRI	[2PW, 2PW + [50, 400) μs)
Costas	bandwidth	[5, 23) MHz
	code length	{3, 4, 5, 6, 8, 9, 10}
Frank	frequency	[3, 23) MHz
	code length	[3, 8]
P1	frequency	[3, 23) MHz
	code length	[3, 8]
Linear chirp	start frequency	[3, 15) MHz
	bandwidth	[2, 23 - start_freq) MHz
Barker	frequency	[3, 23) MHz
	code length	{2, 3, 4, 5, 7, 11, 13}
P3	frequency	[3, 23) MHz
	code length	[3, 20]

C. Training Procedure

Every epoch, a new training set is created to further increase our database artificially. The steps are as follows:

- 1) Randomly draw 3000 pairs of training signals to be mixed from the 6000 simulated waveforms.
- 2) Cut out chunks of size 65280, i.e. the input and output signal lengths of the network, from the saved signals with 10^6 time steps. The position is chosen at random.
- 3) Scale the signals such that they have amplitudes in the range of -10 dBm to -80 dBm.

- 4) Corrupt them by adding Gaussian noise of various levels.
- 5) Mix the signals by adding them together.
- 6) Normalize the mixture and ground truth signals by dividing their amplitudes by the maximum amplitude of the input mixture.

Our test set is built with the same procedure, utilizing all independent and real test samples once. We use the scale-dependent signal-to-distortion ratio (SD-SDR) [17] as training objective, which is defined as

$$\text{SD-SDR}(s, \hat{s}) = 10 \log_{10} \left(\frac{\left\| \frac{\hat{s}^T s}{\|\hat{s}\|^2} s \right\|^2}{\|s - \hat{s}\|^2} \right), \quad (20)$$

where s is the "ground truth" signal in the machine learning sense and \hat{s} its estimate. SD-SDR has shown to provide good separation results while preserving important amplitude information. Utilizing utterance-level Permutation Invariant Training (uPIT) [18], [19] to tackle the output permutation problem that is associated with blind source separation, we get the following loss function $l(s, \hat{s})$

$$l(s, \hat{s}) = - \max_{\pi \in \Pi_C} \frac{1}{C} \sum_{c=1}^C \text{SD-SDR}(s_c, \hat{s}_{\pi(c)}). \quad (21)$$

Π_C is the set of possible output channel permutations with C being the number of channels. This function optimizes the average SD-SDR of both signals. Output channels are permuted such that this objective is maximized. Permutation invariance is necessary, since we have no knowledge about the input waveforms and therefore can't assign certain signals, e.g. chirps, to a fixed network output channel.

We train the models in TensorFlow [20] for 70 epochs, using the adam optimizer [9] with default settings and a decaying learning rate lr defined by the schedule

$$lr = 10^{-4} * 0.90^{epoch}. \quad (22)$$

We also apply the built-in loss scaling, which dynamically scales the loss after a forward pass. This is necessary to solve the problem of rare underflows during backpropagation, caused by the large value range of different signal amplitudes, even when running our network with 32 bit floating point and 64 bit complex precision.

IV. RESULTS

The learning curve of the proposed model can be seen in Fig. 4. It shows a clear performance enhancement over the course of training and converges smoothly. Train and test losses with simulated data are almost equal and the discrepancy between test losses using real and simulated data is expected since real test samples have lower SNR because of attenuation and other hardware effects. The seen behavior can be a result of underfitting¹. If this assumption is correct, a further enlargement of the model size, e.g. by increasing the feature dimension N , could lead to better results. It also

¹Subsequent studies should investigate this by training larger models.

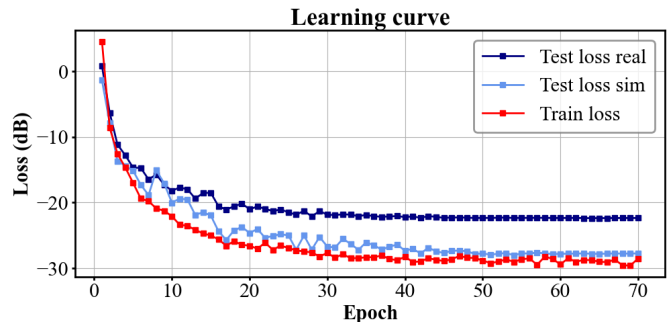


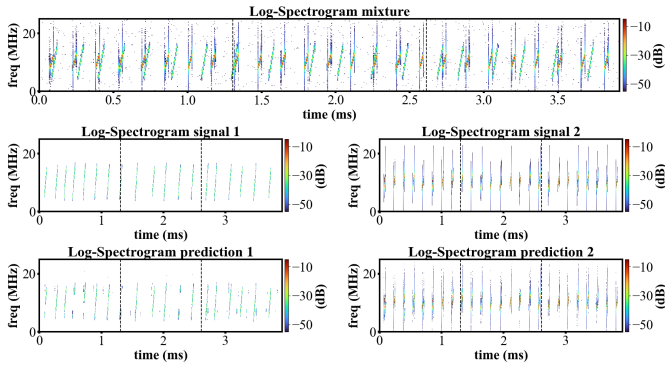
Fig. 4: Train and test losses with real and simulated data evaluated each training epoch.

suggests that we are experiencing a memory bottleneck, mostly driven by the memory complexity of vanilla Transformer Encoders.

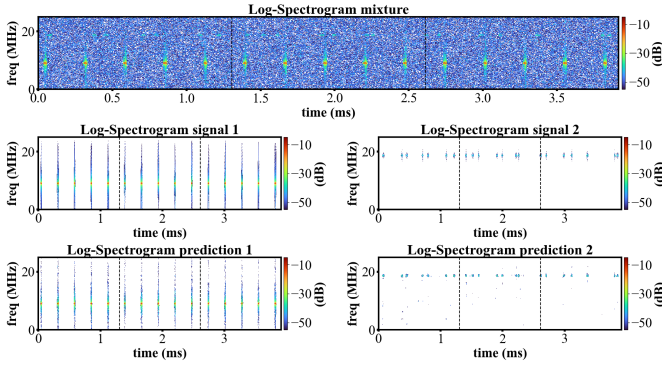
Next, we demonstrate the capabilities of our system through presenting multiple separated test samples in Fig. 5. We stack three observation periods together, each having the length of our model input and outputs. This is done to check for unwanted channel swaps that might occur since we train on restricted input lengths, i.e. one utterance in uPIT, between which output channels can change. Results show, that in none of the examples, channel swaps occur. They happen very rarely in the whole test set, which would require some additional matching or tracking to resolve the issue. Our model is able to separate similar chirps, see Fig. 5a. Remember, that it has not seen any chirp during training. The closest and only frequency modulated waveforms in the training set are Costas codes, which look quite different. Our system also works under low SNR conditions (Fig. 5b), can separate overlapping CW and pulsed waveforms (Fig. 5c) and even functions if only one signal is present (Fig. 5d), which has never been the case during training. Further note the implicit denoising, since the model was trained to predict clean and purely simulated data. Up to some examples where separation fails and which have to be studied in more detail in the future, the given examples are representative and proof the potential of the proposed method, especially given the fact that our training data contains only three different itrapulse modulations.

CONCLUSION

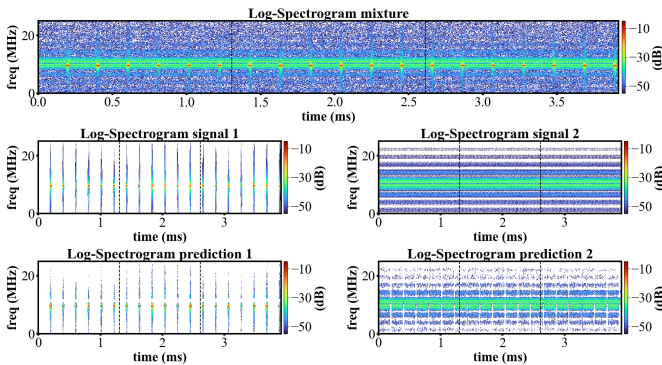
We proposed a new algorithm for the separation of RF signals to overcome the limitations of current deinterleaving methods, which often require the signals to be distinguishable in frequency or AOA. Therefore, a neural network architecture has been developed that separates mixed signals in time domain. We have shown that our model is capable of separating two unknown waveforms with a single input channel and in a defined frequency band under difficult conditions. This might enable us to deal with scenarios, where current methods fail. The network architecture could also be used as a baseline for different tasks with RF signals or modified to separate signals in other domains. For future work, we see multiple



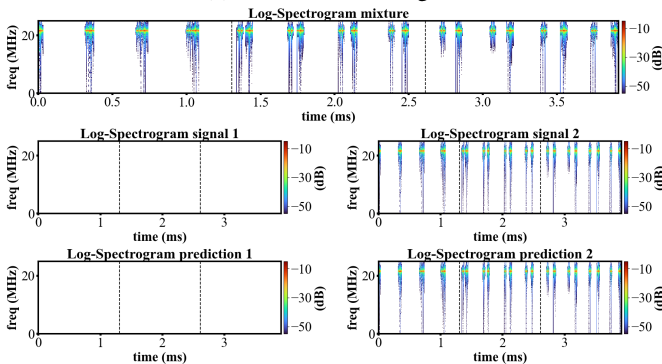
(a) Similar chirps.



(b) Low SNR.



(c) Pulsed and CW signals.



(d) Only one signal.

Fig. 5: Separation under challenging conditions.

research directions. To improve the given model, extending the simulation framework and collecting more labeled training data would likely be most effective. We have shown that memory complexity might be an issue. This becomes even more relevant, if larger bandwidths are to be investigated. Network pruning but especially memory efficient Transformer Encoders could alleviate this problem. Cases where separation fails should be studied in subsequent work. Extending the algorithm to handle an unknown number of signals would make the proposed system applicable to a broader range of problems. Finally, the performance of the system could be compared to classical methods if angular information is available by using multi channel receivers.

ACKNOWLEDGMENT

We would like to thank Angel Slavov for his help with the real data generation.

REFERENCES

- [1] S. Lin, M. Thompson, S. Davezac, and J. C. S. Jr., "Comparison of time of arrival vs. multiple parameter based radar pulse train deinterleavers," in *Signal Processing, Sensor Fusion, and Target Recognition XV* (I. Kadar, ed.), vol. 6235, pp. 561 – 570, International Society for Optics and Photonics, SPIE, 2006.
- [2] O. Can, Y. Z. Gürbüz, B. Yıldırım, and A. A. Alatan, "Blind deinterleaving of signals in time series with self-attention based soft min-cost flow learning," in *ICASSP 2021-2021 IEEE International Conference on Acoustics, Speech and Signal Processing (ICASSP)*, pp. 3295–3299, IEEE, 2021.
- [3] J. R. Hershey, Z. Chen, J. Le Roux, and S. Watanabe, "Deep clustering: Discriminative embeddings for segmentation and separation," in *2016 IEEE International Conference on Acoustics, Speech and Signal Processing (ICASSP)*, pp. 31–35, IEEE, 2016.
- [4] Y. Luo and N. Mesgarani, "Conv-tasnet: Surpassing ideal time-frequency magnitude masking for speech separation," *IEEE/ACM transactions on audio, speech, and language processing*, vol. 27, no. 8, pp. 1256–1266, 2019.
- [5] Y. Luo, Z. Chen, and T. Yoshioka, "Dual-path rnn: efficient long sequence modeling for time-domain single-channel speech separation," in *ICASSP 2020-2020 IEEE International Conference on Acoustics, Speech and Signal Processing (ICASSP)*, pp. 46–50, IEEE, 2020.
- [6] C. Subakan, M. Ravanelli, S. Cornell, M. Bronzi, and J. Zhong, "Attention is All You Need in Speech Separation," *arXiv e-prints*, p. arXiv:2010.13154, Oct. 2020.
- [7] J. Smith, S. U. C. for Computer Research in Music, Acoustics, and S. U. D. of Music, *Spectral Audio Signal Processing*. W3K, 2011.
- [8] F. Chollet, *Deep Learning with Python*. USA: Manning Publications Co., 1st ed., 2017.
- [9] I. Goodfellow, Y. Bengio, and A. Courville, *Deep Learning*. MIT Press, 2016. <http://www.deeplearningbook.org>.
- [10] J. L. Ba, J. R. Kiros, and G. E. Hinton, "Layer normalization," *arXiv preprint arXiv:1607.06450*, 2016.
- [11] A. Vaswani, N. Shazeer, N. Parmar, J. Uszkoreit, L. Jones, A. N. Gomez, Ł. Kaiser, and I. Polosukhin, "Attention is all you need," *Advances in neural information processing systems*, vol. 30, 2017.
- [12] Z. Shi, R. Liu, and J. Han, "Lafurca: Iterative refined speech separation based on context-aware dual-path parallel bi-ilstm," *arXiv preprint arXiv:2001.08998*, 2020.
- [13] J. Chen, Q. Mao, and D. Liu, "Dual-path transformer network: Direct context-aware modeling for end-to-end monaural speech separation," *arXiv preprint arXiv:2007.13975*, 2020.
- [14] V. Dumoulin and F. Visin, "A guide to convolution arithmetic for deep learning," *arXiv preprint arXiv:1603.07285*, 2016.
- [15] GNU Radio. <https://www.gnuradio.org/>, accessed April 2022.
- [16] N. Levanon and E. Mozeson, *Radar Signals*. John Wiley & Sons, Inc., Hoboken, New Jersey, 2004.

- [17] J. Le Roux, S. Wisdom, H. Erdogan, and J. R. Hershey, “Sdr–half-baked or well done?,” in *ICASSP 2019-2019 IEEE International Conference on Acoustics, Speech and Signal Processing (ICASSP)*, pp. 626–630, IEEE, 2019.
- [18] M. Kolbæk, D. Yu, Z.-H. Tan, and J. Jensen, “Multitalker speech separation with utterance-level permutation invariant training of deep recurrent neural networks,” *IEEE/ACM Transactions on Audio, Speech, and Language Processing*, vol. 25, no. 10, pp. 1901–1913, 2017.
- [19] E. Nachmani, Y. Adi, and L. Wolf, “Voice separation with an unknown number of multiple speakers,” in *International Conference on Machine Learning*, pp. 7164–7175, PMLR, 2020.
- [20] M. Abadi, A. Agarwal, P. Barham, E. Brevdo, Z. Chen, C. Citro, G. S. Corrado, A. Davis, J. Dean, M. Devin, S. Ghemawat, I. Goodfellow, A. Harp, G. Irving, M. Isard, Y. Jia, R. Jozefowicz, L. Kaiser, M. Kudlur, J. Levenberg, D. Mané, R. Monga, S. Moore, D. Murray, C. Olah, M. Schuster, J. Shlens, B. Steiner, I. Sutskever, K. Talwar, P. Tucker, V. Vanhoucke, V. Vasudevan, F. Viégas, O. Vinyals, P. Warden, M. Wattenberg, M. Wicke, Y. Yu, and X. Zheng, “TensorFlow: Large-scale machine learning on heterogeneous systems,” 2015. Software available from tensorflow.org.